PHYSICAL REVIEW D **85,** 044016 (2012)

Observational cosmology using characteristic numerical relativity: Characteristic formalism on null geodesics

P. J. van der Walt[1] and N. T. Bishop[1]

[1]*Department of Mathematics, Rhodes University, Grahamstown 6140, South Africa*

(Received 25 November 2011; published 7 February 2012)

The characteristic formalism of numerical relativity is based on a system of coordinates aligned with outgoing null cones. While these coordinates were designed for studying gravitational waves, they can also be easily adapted to model cosmological past null cones (PNCs). Similar to observational coordinates in the observational approach to cosmology, this then provides a model that only makes use of information causally connected to an observer. However, the diameter distance, which is used as a radial coordinate, limits the model's cosmological application to the region prior to the PNC refocusing. This is because after refocusing, the diameter distance ceases to be a unique measure of distance. This paper addresses the problem by introducing a metric based on the Bondi-Sachs metric where the radial coordinate is replaced by an affine parameter. A model is derived from this metric and it is then shown how an existing numerical scheme can be adapted for simulation of cosmological PNC behavior. Numerical calculations on this model are found to have the same stability and convergence properties as the standard characteristic formalism.

DOI: 10.1103/PhysRevD.85.044016 PACS numbers: 04.25.D−, 98.80.Jk

I. INTRODUCTION

The observational approach to cosmology is the endeavor to reconstruct the geometry of the Universe using observations that do not require the prior assumption of a cosmological model. Using this approach, it was shown in [1] that given ideal cosmological observations, the only essential assumption necessary to determine the geometry of the Universe is a theory of gravity. Assuming General Relativity, then, the full set of Einstein field equations (EFEs) can be used to reconstruct the geometry of the Universe using direct observations on the past null cone (PNC) as boundary conditions. Observationally and theoretically this is a very ambitious task and therefore, current developments have been restricted to spherically symmetric dust models while only relaxing the usual assumption of homogeneity in the radial direction. These restricted models are important for the development of theoretical foundations and also useful as verification models since they avoid the circularity of verifying what has already been assumed. For instance, doing investigations such as quantifying homogeneity on different scales, testing the verifiability of cosmology [1], validating the Copernican principle [2] and determining the metric of the Universe [3] require more general models than the conventional Robertson-Walker geometries.

The *Observational Cosmology* (OC) program of Ellis and others played an instrumental part in the development of the observational approach. Of particular interest is their use of observer coordinates which is based on the optical coordinates of Temple [4]. These coordinates are based on the natural propagation of electromagnetic radiation and follow the causal structure of an observer PNC. This approach then consists of two problems: first, astronomical observations are used to set up the metric on the local PNC and second, these form the final values of a characteristic final value problem which determines the historical evolution of the region causally connected to the PNC (i.e. the interior of the PNC). The PNC and its interior, which is the causally connected region of a cosmological observer, is of fundamental importance since it defines the limits on which cosmological models can be validated from direct observations. Apart from the initial *Ideal Observational Cosmology* report [1], which focused on the fundamental principles, the focus of the OC program has mostly been on exact solutions and perturbations using tetrad formalisms in spherical symmetry. Some recent developments are presented in [5–7] and a summary in [8]. Numerical algorithms have been proposed in [3] using a metric-based approach but these have not been implemented. A separate line of development based on the Lemaître-Tolman-Bondi (LTB) model, using comoving coordinates, using the models introduced in [9,10], was followed in [11,12] to reconstruct the observer metric numerically. Some important aspects addressed in the LTB approach are the treatment of a reconverging PNC through coordinate singularities and the sensitivity of the numerics when using realistic data as boundary conditions.

The characteristic formalism of numerical relativity [13–15] usually associated with studying gravitational waves, was put forward in [16,17] as a method for modeling the observable universe. With the motivation that there exists a well-established base of null-cone numerical schemes, it was investigated to what extent these can be employed to simulate the evolution into the past of a cosmological PNC, instead of modeling the evolution into the future of a future null cone. It was found that with minor cosmological considerations, this method was

 © 2012 American Physical Society

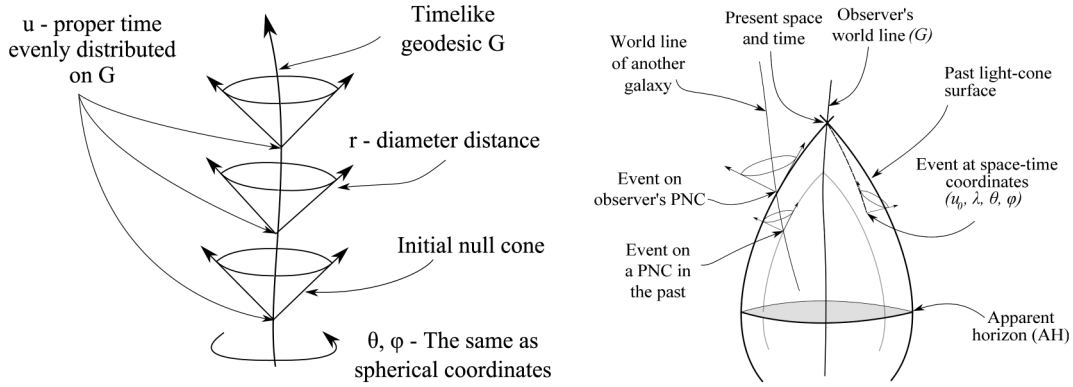

FIG. 1. On the left-hand side, the null coordinates of the characteristic formalism and on the right-hand side, the affine null-cone coordinates for cosmology.

very well suited for modeling the historical evolution of the observable universe. That is apart from a known limitation of the characteristic formalism; i.e. in modeling the reconvergence of the PNC of an expanding universe, the diameter distance, as radial coordinate, becomes multivalued and limits the feasible radial extent of this formalism to the region prior to the observer apparent horizon (AH). Since the properties of the observable universe at the AH are directly related to the cosmological constant (Λ) [3,6,18], extending the model beyond the AH is a compulsory requirement for studying contemporary problems in cosmology.

This paper addresses this problem by introducing a metric based on the Bondi-Sachs metric where the radial coordinate is replaced with an affine parameter. We derive the model with a cosmological constant Λ incorporated into the Einstein field equations, and regard Λ as a parameter of the theory of gravity rather than as a matter source term. Similar to the conventional characteristic formalism, this model consists of a system of differential equations for numerically evolving the EFEs as a characteristic initial value problem (CIVP). A numerical code implemented for the method has been found to be second-order convergent. This code enables simulations of different models given identical data on the initial null cone and provides a method to investigate their physical consistency within the causally connected region of our current PNC. These developments closely follow existing 3D schemes developed for gravitational wave simulations, which should make it natural to extend the affine CIVP beyond spherical symmetric simulations.

In Sec. II, an affine parameter is introduced in the Bondi-Sachs metric to derive the affine CIVP model for cosmology. Details of the numerical implementation are given in Sec. III and coordinate transformations, which relate comoving coordinates to the affine CIVP coordinates are discussed in Sec. IV. Results of simulations with the new coordinates are presented in Sec. V. Section VI concludes the paper.

II. CHARACTERISTIC FORMALISM ON NULL GEODESICS

A. Characteristic formalism with affine radial coordinate

The conventional characteristic formalism in numerical relativity uses a frame of reference based on outgoing null cones that evolve from values on an initial null cone. The idea is conceptualized in Fig. 1. G is a timelike geodesic, and u is the proper time on G. (In practice, in numerical relativity simulations the inner boundary of the null cone is usually a timelike worldtube rather than a geodesic, but the problem can be formulated with a geodesic). Null geodesics emanating from G have constant (u, θ, φ), and near G the angular coordinates θ and φ have the same meaning as in spherical polar coordinates. The coordinate r is the diameter, or area, distance defined by the condition that the surface area of a shell of constant r is $4\pi r^2$.

The geometry of the characteristic formalism is described by the Bondi-Sachs metric, which in spherical symmetry is formulated as[1]

$$ds^2 = -e^{2\beta}\left(1 + \frac{W}{r}\right)du^2 - 2e^{2\beta}dudr + r^2\{d\theta^2 + \sin^2\theta d\varphi^2\}. \quad (1)$$

This can be recognized as a generalization of the well-known Eddington-Finkelstein form of the exterior Schwarzschild metric, obtained by setting $\beta = 0$, $W = -2M$, where M is the mass of the source. The coordinate system is defined such that β and W vanish at the vertex of each null cone, i.e. at $r = 0$ Eq. (1) reduces to a Minkowskian metric.

Starting with the Bondi-Sachs metric (1), an affinely parameterized geodesic in these coordinates is determined through

[1]The notation used here is based on that of [13] and substituting $W = V - r$ will give the original notation of Bondi and Sachs in [19–21].

$$\frac{d^2r}{d\lambda^2} + \Gamma^1_{11}\left(\frac{dr}{d\lambda}\right)^2 = 0 \Rightarrow \frac{d^2r}{d\lambda^2} + 2\beta_{,r}\left(\frac{dr}{d\lambda}\right)^2 = 0. \quad (2)$$

Setting $\lambda = r$ at the origin provides the initial conditions $r(0) = \lambda(0) = 0$ and $dr/d\lambda|_{\lambda=0} = 1$ then solving gives

$$\frac{dr}{d\lambda} = e^{-2\beta}. \quad (3)$$

Using tensor transformation laws and substituting (3) for all $\partial r/\partial\lambda$ terms, a new metric with the radial coordinate λ is introduced as

$$ds^2 = -\left(1 + \frac{\hat{W}}{\hat{r}}\right)du^2 - 2du d\lambda + \hat{r}^2\{d\theta^2 + \sin^2\theta d\varphi^2\}$$
$$\text{with: } \hat{W} = \hat{W}(u, \lambda) \quad \text{and} \quad \hat{r} = \hat{r}(u, \lambda). \quad (4)$$

Substituting (4) into the EFEs, using the form $R_{ab} = \kappa(T_{ab} - \frac{1}{2}Tg_{ab}) + \Lambda g_{ab}$, with the stress-tensor for a dust-like fluid ($T_{ab} = \rho v_a v_b$ and $T = -\rho$) gives[2]

$$\hat{r}_{,\lambda\lambda} = -\frac{1}{2}\kappa\hat{r}\rho(v_1)^2 \quad (5)$$

$$\hat{r}_{,u\lambda} = \frac{1}{2}\left\{\hat{W}_{,\lambda}\hat{r}_{,\lambda} + \hat{r}\hat{r}_{,\lambda\lambda} + \hat{W}\hat{r}_{,\lambda\lambda} - 2\hat{r}_{,u}\hat{r}_{,\lambda} - 1 + (\hat{r}_{,\lambda})^2 + \frac{1}{2}\kappa\rho\hat{r}^2 + \Lambda\hat{r}^2\right\}\Big/\hat{r} \quad (6)$$

$$\hat{W}_{,\lambda\lambda} = \frac{\hat{W}}{\hat{r}}\hat{r}_{,\lambda\lambda} + 4\hat{r}_{,u\lambda} + 2\kappa\left(v_0 v_1\rho - \frac{1}{2}\rho\right)\hat{r} - 2\Lambda\hat{r} \text{ with: } \hat{r}(0) = \hat{W}(0) = \hat{W}_{,\lambda}(0) = \hat{r}_{,u}(0) = 0 \text{ and } \hat{r}_{,\lambda}(0) = 1. \quad (7)$$

Further, substituting the dust stress-tensor and (4) into the continuity equation, $T^{ab}_{;b} = 0$, the energy-momentum equations follow

$$v_{1,u} = \frac{1}{v_1}\left\{(\hat{V}_w v_1 - v_0)v_{1,\lambda} + \frac{1}{2}(v_1)^2\hat{V}_{w,\lambda}\right\} \quad (8)$$

$$\rho_{,u} = \frac{1}{v_1}\left\{\rho\left[\hat{V}_w\left(\frac{2v_1}{\hat{r}}\hat{r}_{,\lambda} + v_{1,\lambda}\right) - \left(\frac{2v_0}{\hat{r}}\hat{r}_{,\lambda} + v_{0,\lambda}\right) + \hat{V}_{w,\lambda}v_1 - \left(\frac{2\hat{r}_{,u}}{\hat{r}}\right)v_1\right] + \rho_{,\lambda}(\hat{V}_w v_1 - v_0) - \rho v_{1,u}\right\}$$
$$\text{with: } \hat{V}_w = 1 + \frac{\hat{W}}{\hat{r}}. \quad (9)$$

Making use of the normalization condition, $g^{ab}v_a v_b = -1$, v_0 can be written in terms of v_1 as

$$v_0 = \frac{1}{2}\hat{V}_w v_1 + \frac{1}{2}v_1^{-1}. \quad (10)$$

[2]Using geometric units $G = 1$, $c = 1$ and $\kappa = 8\pi$

Having the values on the initial null cone for ρ and v_1, Eqs. (5) to (10) form a hierarchical system that can be solved in the order (5)–(7) and (10), then solving Eqs. (8) and (9) evolves the system to the next null cone where the process can be repeated until the domain of calculation has been covered. These equations are all interdependent and require an iterative scheme for a numerical solution.

B. Cosmological considerations

The model introduced in Sec. II A is essentially a null-cone formalism which makes provision for a null cone that can reconverge at some distance from the cone vertex. Taking G to be the worldline of an observer located at the cone vertex and integrating into the past, these coordinates can be naturally aligned with a cosmological PNC. Further, it being spherically symmetric and radially inhomogeneous, classifies it as a LTB model in null coordinates. Using this model, the simulations done in [16,17] can be extended beyond the apparent horizon (AH). Figure 1 illustrates the differences between conventional characteristic coordinates and the affine coordinates. Besides being not comoving, the affine coordinates closely resemble the observer coordinates as described in [1].

As an observational cosmology problem, where the geometry is determined from direct observations, there are two subproblems to be solved:

(i) Reconstruct the geometry of the local PNC from directly observable quantities, such as redshift-distance and galaxy number counts.
(ii) Evolve the model as a reverse CIVP to determine the interior of the PNC using the values determined in (i) as initial conditions.

Although the accumulation of cosmological data in recent years has been astounding, these are not yet sufficiently complete for a practical implementation of the first problem, which will have to incorporate aspects such as data reduction and the sensitivity of the model to observational errors. These aspects will not be considered in this paper and only a conceptual description of the relations between observable quantities and the required input for the model will be described in the next section. The second subproblem will be treated in detail in the remainder of the paper through the development of a numerical code for the affine CIVP model. By itself this provides a mechanism for testing hypothesised models by evaluating the behavior of their PNCs under given initial values. The PNC behaviors of different models given similar initial values are particularly interesting cases to investigate.

C. Reconstructing the metric

As initial data for the model, $v_1(\lambda)$ and $\rho(\lambda)$ have to be determined from observations on the PNC. These require measures of the radial distribution of expansion and density. As a measure of expansion, redshift in terms of the luminosity distance (d_L) can be determined from

redshift-magnitude observations (e.g. type Ia supernovae observations). The reciprocity theorem can then be used to convert d_L-redshift to diameter distance-redshift relations (see [22])

$$z(d_L) \quad \text{and} \quad d_L = (1+z)^2 r_0 \Rightarrow \hat{z} = z(r_0). \tag{11}$$

Here the zero subscript refers to a value on the current PNC. The redshift is directly related to the time component of the contravariant velocity:

$$1 + \hat{z} = \frac{du}{d\tau} = v^0, \tag{12}$$

where τ is the proper time along general galactic world lines (see [1]). This can be used to determine the covariant velocity v_1:

$$v_1(r_0) = -v^0 = -(1+\hat{z}). \tag{13}$$

As a measure of density, observed galaxy number counts (n) in terms of z can be used to determine $\rho(r_0)$. Galaxy redshift surveys can provide data for this, although current surveys are not yet sufficiently complete at high redshifts. Since $\hat{z}(r_0)$ is known, $n(z)$ can be rewritten as $\hat{n}(r_0) = n(\hat{z}(r_0))$. It was shown in [16] that the proper number count can be written as

$$N = \frac{n}{(1+z)}. \tag{14}$$

In terms of the diameter distance, the proper number count then becomes

$$\hat{N}(r_0) = \frac{\hat{n}}{(1+\hat{z})}. \tag{15}$$

The proper density is then related to the proper number count

$$\rho(r_0) = f(\hat{N}). \tag{16}$$

The details of this relation will not be considered at this stage but in principle it must take into account aspects such as dark matter and source evolution, preferably with factors independent of an already assumed cosmological model.

From (13) and (16) the required values of ρ and v_1 are obtainable in terms of the diameter distance. Since these are required in terms of λ, interchanging the independent variable in (5) provides a method to relate λ in terms of r. Starting with (5), rewritten as a system of ordinary differential equations (ODEs), introducing $\hat{S}$,

$$\hat{r}_{,\lambda} = \hat{S} \tag{17}$$

$$\hat{S}_{,\lambda} = \hat{r}_{,\lambda\lambda} = -\frac{1}{2}\kappa\hat{r}\rho(v_1)^2 \quad \text{with: } \hat{r}(0) = 0 \text{ and } \hat{S}(0) = 1, \tag{18}$$

then interchanging the roles of λ and r, simplifying, rearranging and introducing $\hat{U}$ provides ODE expressions for $\lambda_{,\hat{r}\hat{r}}$

$$\lambda_{,\hat{r}} = \hat{U} \tag{19}$$

$$\hat{U}_{,\hat{r}} = \lambda_{,\hat{r}\hat{r}} = \left(\frac{1}{2}\kappa\hat{r}\rho(v_1)^2\right)\hat{U}^3 \quad \text{with: } \lambda(0) = 0 \text{ and } \hat{U}(0) = 1. \tag{20}$$

Although these equations will not be solved at this stage, there are some complications that will require special consideration around the AH. These arise from the fact that the diameter distance in an expanding universe is not necessarily monotonically increasing and therefore, not a unique independent variable. In these cases, $\hat{r}$ reaches a maximum and then decreases. At the maximum diameter distance, the AH, $\hat{r}_{,\lambda} = 0$, and $\lambda_{,\hat{r}}$ is singular. In general, this can be overcome by separating the solution into regions prior, around and succeeding the AH where the region around the AH is solved using series expansions. Such a method was previously implemented in [11] to handle singularities around the AH for LTB models.

It should be noted that [18], followed by [3,6], derived a relationship for the cosmological constant Λ (which we are regarding as a parameter of the theory of gravity) involving the maximum value of $\hat{r}$ and matter data within the PNC. In order to test the theory of gravity more generally, a measurement involving a rate of change over time is required. Redshift drift $z_{,u}(z)$ [2], which is one of the design objectives of the CODEX spectrograph planned for the European Extremely Large Telescope (E-ELT) [23], can be used for this purpose. From (13) we have

$$v_1(r_0) = -(1+\hat{z}) \Rightarrow v_{1,u}(r_0) = -\hat{z}_{,u}(\hat{z}), \tag{21}$$

and then an evaluation of the difference between the left- and right-hand sides of Eq. (8) provides a test of the theory being used.

In the LTB models investigated in [11,12], data reduction methods were introduced which provide valuable insight into the methodology of converting realistic data into useful initial data. In combination with the methods introduced in this section, all options will have to be considered when data of sufficient completeness becomes available for observational models.

III. NUMERICAL IMPLEMENTATION

The numerical scheme described here is in structure similar to the finite difference scheme described in [17], which in turn was based on the general 3D code developed in [13,24]. Since the original scheme is based on first-order ODEs, the second-order hypersurface equations are rewritten by introducing $\hat{R}(u,\lambda) = \hat{r}_{,u}$, $\hat{S}(u,\lambda)$, and $\hat{T}(u,\lambda)$, which then gives:

$$\hat{r}_{,\lambda} = \hat{S} \tag{22}$$

$$\hat{S}_{,\lambda} = \hat{r}_{,\lambda\lambda} = -\frac{1}{2}\kappa\hat{r}\rho(v_1)^2 \tag{23}$$

$$\hat{R}_{,\lambda} = \hat{r}_{,u\lambda} = \frac{1}{2}\left\{\hat{T}\hat{S} + \hat{r}\hat{S}_{,\lambda} + \hat{W}\hat{S}_{,\lambda} - 2\hat{R}\hat{S} - 1 + \hat{S}^2 + \frac{1}{2}\kappa\rho\hat{r}^2 + \Lambda\hat{r}^2\right\}\Big/\hat{r} \tag{24}$$

$$\hat{W}_{,\lambda} = \hat{T} \tag{25}$$

$$\hat{T}_{,\lambda} = \hat{W}_{,\lambda\lambda} = \frac{\hat{W}}{\hat{r}}\hat{S}_{,\lambda} + 4\hat{R}_{,\lambda} + 2\kappa\left(v_0 v_1 \rho - \frac{1}{2}\rho\right)\hat{r} - 2\Lambda\hat{r}$$
$$\text{with: } \hat{r}(0) = \hat{W}(0) = \hat{R}(0) = \hat{T}(0) = 0 \quad \text{and} \quad \hat{S}(0) = 1. \tag{26}$$

These equations can be solved using standard ODE methods for systems of equations where (22) and (23) are solved as one system and (24)–(26) are solved as a separate system. In both cases a number of iterations are required to obtain convergence.

The discretization strategy followed is based on a rectangular grid similar to the one used in [17] but using λ as the radial coordinate. Solving the hypersurface equations is done with a central difference method on half steps between the r-grid points, using

$$g^i_j = g^i_{j-1} + \frac{\Delta\lambda}{2}(g^i_{,rj} + g^i_{,rj-1}) \tag{27}$$

with i being the time step and j the radial step. Here, $g^i_{,rj}$ is calculated by substituting known values into Eqs. (22)–(26). In order to solve the evolution equations, (8) and (9), their general form is notated as

$$v_{1,u} = F_{v1} \quad \text{and} \quad \rho_{,u} = F_\rho \tag{28}$$

and as explicit finite differences on a time half-step they are written as

$$v^{n+1}_{1j} = v^n_{1j} + \Delta u F^{n+1/2}_{v1j} \quad \text{and} \quad \rho^{n+1}_j = \rho^n_j + \Delta u F^{n+1/2}_{\rho j}. \tag{29}$$

Here, n is a time iterator that will approach i. In these equations, the numerical values at the point (i, j) are used to evaluate the matter terms and hypersurface derivatives. Radial matter derivatives are calculated making use of standard central difference formulae (see for instance [25] p. 160–161).

After setting up a suitable grid, the numerical algorithm can be summarized in the following steps:

(i) Set the ρ and v_1 initial values on to the initial grid points. These values will, in principle, be obtained from observations.

(ii) Calculate r, $r_{,u}$, W and v_0 from ρ and v_1 on the initial null cone using (22)–(26).

(iii) Calculate F^n_j, with $n = 1$ for the initial step, from the values of v_1, ρ, r, $r_{,u}$, W, and v_0 using (28).

(iv) Set $F^{n+1/2}_j = F^n_j$, again $n = 1$ for the initial step, and calculate v_1 and ρ as an initial approximation that will approach the actual values with subsequent iterations using (29).

(v) Use the new values of v_1 and ρ to calculate r, $r_{,u}$, W, and v_0 and their radial derivatives similar to (ii).

(vi) Calculate $F^{n+1/2}_j = 1/2(F^n_j + F^{n+1}_j)$ from values in (v) and again v_1 and ρ for F^{n+1}_j and the values in (iii) for F^n_j.

(vii) Test the calculations in (vi) for accuracy and convergence. If they are sufficiently accurate, move to the next time step, otherwise repeat steps (v) and (vi) with the new values of v_1 and ρ.

As with the standard characteristic model, described in [16,17], calculations in the regions around $\lambda = 0$ require special consideration. The mechanisms used in [17] for these regions was directly adapted for the affine CIVP model. In the $\lambda \approx 0$ region, it is evident from the occurrence of λ denominators that Eqs. (8) and (9) will not be well-behaved. Consequently, the $\lambda \approx 0$ region is calculated by making use of second-order series expansions. The region where the series solution meets with the CIVP solution, also requires special treatment to avoid artificial instabilities. This has been done by smoothing out the merger region with a weighted average between the two solutions.

IV. TRANSFORMATIONS: COMOVING COORDINATES

A. General transformation

As a measure of the degree of convergence and accuracy, numerical calculations have to be compared with results from known solutions, which require coordinate transformations from conventional comoving cosmological coordinates to affine null coordinates. These transformations follow directly from calculating the geodesic paths in space and time. This has the general form

$$\frac{d^2x^a}{d\lambda^2} + \Gamma^a_{bc}\frac{dx^b}{d\lambda}\frac{dx^c}{d\lambda} = 0. \tag{30}$$

The parabolic LTB model, which is spherically symmetric and radially inhomogeneous, will be used as the general case for transformations. Its geometry in comoving synchronous coordinates is described by the metric[3]

$$ds^2 = -dt^2 + [R_{,r}(t,r)]^2 dr^2 + [R(t,r)]^2\{d\theta^2 + \sin^2\theta d\varphi^2\}. \tag{31}$$

Here, t is the cosmic (proper) time, r is a comoving radial coordinate with θ and φ the inclination and azimuth

[3]Note that r here is the comoving radial distance and not the diameter distance.

angles. $R(t, r)$ is the areal radius and $4\pi R^2$ defines the proper surface area of a sphere with coordinate radius r at a constant time slice [26].

Using (30), the geodesic equations for the LTB model becomes

$$\frac{d^2t}{d\lambda^2} + \Gamma^0_{11}\left(\frac{dr}{d\lambda}\right)^2 = 0 \tag{32}$$

$$\frac{d^2r}{d\lambda^2} + 2\Gamma^1_{01}\frac{dt}{d\lambda}\frac{dr}{d\lambda} + \Gamma^1_{11}\left(\frac{dr}{d\lambda}\right)^2 = 0. \tag{33}$$

When scaled to some maximum time, t_0, as the current age of a universe, the conditions at $\lambda = 0$ are $t = t_0$ and $r = 0$ with the initial directions constrained to be null by $dt/d\lambda = 1$ and $dr/d\lambda = 1/R_{,r}(t_0, 0)$. As comparative values on a null-cone grid, the covariant velocity follows directly from $v_1 = dt/d\lambda$, the diameter distance from $\hat{r}(\lambda) = R[t, r(\lambda)]$, while ρ is determined from the coordinate expression for the specific model using $[t(\lambda), r(\lambda)]$ as the coordinates for t and r on a null cone.

B. Models for code verification

1. Einstein-de Sitter model

As an illustration of comoving to affine transformations, the Einstein-de Sitter (EdS) model, scaled to $t_0 = 1$ with $G = 1$, which has the metric

$$ds^2 = -dt^2 + t^{4/3}dr^2 + t^{4/3}r^2\{d\theta^2 + \sin^2\theta d\varphi^2\}. \tag{34}$$

provides a system of equations from which $t(\lambda)$ and $r(\lambda)$ can be obtained

$$\frac{d^2t}{d\lambda^2} + \frac{2}{3}t^{1/3}\left(\frac{dr}{d\lambda}\right)^2 = 0 \tag{35}$$

$$\frac{d^2r}{d\lambda^2} + \frac{4}{3}t^{-1}\frac{dt}{d\lambda}\frac{dr}{d\lambda} = 0. \tag{36}$$

At $\lambda = 0$: $t = 1$, $r = 0$, $dt/d\lambda = -1$, and $dr/d\lambda = t^{-2/3}$.

Solving these equations numerically provides a useful example of the motivation for working with an affinely parameterized radial coordinate as opposed to the diameter distance. This is illustrated in Fig. 2 where the diameter distance and affine parameter is plotted against the redshift. In terms of observations, with the emphasis on the AH at $z = 1.25$, the diameter distance reaches its maximum and then decreases while λ keeps on increasing and provides a unique coordinate for higher redshifts.

Substituting $t(\lambda)$ into the density equation $\rho = 1/(6\pi t^2)$ provides the density profile on a specific null cone. It is interesting to point out here that as t varies with λ on each null cone, ρ also varies i.e. even though the EdS model is homogeneous in conventional cosmological coordinates, null cones are not hypersurfaces of radial homogeneity and the model becomes inhomogeneous in null coordinates (see [27]).

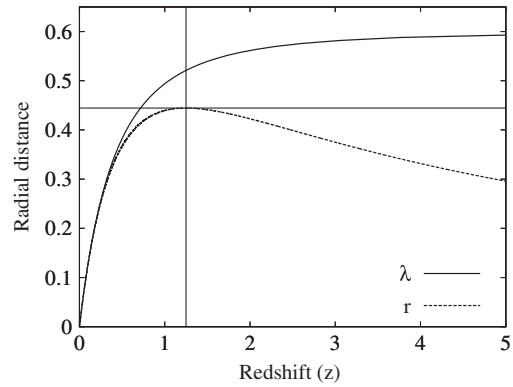

FIG. 2. The radial distance coordinates d_D and λ related to z, which is a common observational measure.

2. ΛCDM

The ΛCDM or concordance model is of interest for the current understanding of the Universe and is also useful to test the affine CIVP model with a nonzero cosmological constant. In terms of the LTB metric (31), using cosmological properties at the current epoch (t_0), the solution of the flat ΛCDM model is (see [28]):

$$R(t, r) = A(t)r = \left(\frac{\Omega_{m0}}{\Omega_\Lambda}\right)^{1/3}\left(\sinh\left[\frac{3}{2}H_0\sqrt{\Omega_\Lambda}t\right]\right)^{2/3}r \tag{37}$$

with the age of the Universe:

$$t_0 = \frac{2}{3}(H_0\sqrt{\Omega_\Lambda})^{-1}\sinh^{-1}\left[\left(\frac{\Omega_\Lambda}{\Omega_{m0}}\right)^{1/2}\right] \tag{38}$$

and the density distribution

$$\rho_m = \frac{3H_0^2}{8\pi G}\frac{\Omega_{m0}A_0^3}{A^3}. \tag{39}$$

Here, Ω_{m0} and Ω_Λ are the current density parameters for baryonic matter and the cosmological constant, respectively, and H_0 is the current Hubble constant. Values representative of the actual Universe are: $\Omega_{m0} = 0.3$, $\Omega_\Lambda = 0.7$ and $H_0 = 72\ \mathrm{Mpc\,s^{-1}\,km^{-1}}$. For the purpose of code verification, however, using geometric units ($G = 1$) and rescaling time to have $t_0 = 1$, a dimensionless value of $H_0 = 0.964$ was used to make comparison with other models more convenient.

3. Lemaître-Tolman-Bondi

LTB models, introduced in [29–31], have been popular in recent years to demonstrate how inhomogeneities can reproduce the effects of type Ia supernovae redshift dimming without the need of a cosmological constant (see [32–36] among others). It, therefore, has physical significance and also provides a general case for testing the effect of radial inhomogeneity on the null-cone behavior. The test cases investigated, here, are for simplicity restricted to the

parabolic solution. Substituting (31) into the EFEs and solving gives (see [10,37]):

$$R(t,r) = \left[\frac{9}{2}M(r)(t - t_B(r))^2\right]^{1/3} \quad \text{and} \quad \rho(t,r) = \frac{M_{,r}}{4\pi R^2 R_{,r}}. \tag{40}$$

$M(r)$ is the *active gravitational mass* which is the mass contributing to the gravitational field and $t_B(r)$ is defined as the *bang time function*, which is a surface defined by the local time at which $R = 0$. A simplified subset of models with mathematical convenient properties follow by setting $M(r) = M_0 r^3$ as a coordinate condition where M_0 is a constant which for illustrative purposes is set to $2/9$. Equations (40) then reduce to:

$$R(t,r) = r(t - t_B(r))^{2/3} \tag{41}$$

with ρ:

$$\rho(t,r) = \frac{1}{2\pi(t - t_B(r))(3t - 3t_B(r) - 2rt_{B,r}(r))}. \tag{42}$$

By selecting $t_B(r) = 0$, Eq. (42) becomes the EdS model, which can be verified against the results in Sec. IV B 1. If $t_B(r) \neq 0$ and $t_{B,r}(r) = 0$, the time of the initial singularity is adjusted and the age of the Universe changes. For nonconstant functions, the initial singularity becomes a singular surface and the age of the Universe becomes subject to the position of an observer (i.e. the age of the Universe depends on r). Thus, a variety of models can be generated for testing the code on parabolic spatial sections.

A simple choice of the bang function is implemented as a verification model:

$$t_B(r) = br, \tag{43}$$

with b being a constant. This simplifies Eqs. (41) and (42) to:

$$R(t,r) = r(t - br)^{2/3} \tag{44}$$

$$\rho(t,r) = \frac{1}{2\pi(t - br)(3t - 5br))}. \tag{45}$$

By varying the value of b, different aspects of inhomogeneity can be studied. The value $b = 0$ is exactly the EdS model and $b > 0$ shifts the age of a universe to a younger age as r increases while $b < 0$ provides the opposite effect where a universe is shifted to an older age as r increases. The latter case is particularly interesting since it provides a mechanism to mimic a cosmological constant on low redshifts [32]. This is, however, not necessarily the case for high redshifts and the case where $b = -0.5$ is used as a model where the effect of inhomogeneity is clearly visible on higher redshifts.

TABLE I. Affine CIVP test cases.

Model	z at $r_{\max}$	$z_{\max}$	u_0	$u_{\max}$	Figures
EdS	1.25	4.5	1	0.35	3 and 4
ΛCDM ($\Omega_\Lambda = 0.7$) [a]	1.61	6	1	0.4	5 and 6
LTB ($b = -0.5$)	1.02	1.2	1	0.2	7 and 8

[a]This result is in agreement with that of [38]

V. RESULTS

A. Verification results

The results of numerical calculations of the models described in Sec. IV B are presented in this section. It is shown how the diameter distance ($\hat{r}$), the covariant velocity (v_1) and the density ρ evolve on PNCs in the past from observations on the current PNC. Also of interest is the evolution of $\hat{r}$ against the redshift z, which provides an illustration of an observer's perception of distance from a particular PNC vertex. In the results the current PNC values are indicated with u_0, the oldest PNC with $u_{\max}$ and an intermediate PNC is also shown between these values. Since the purpose of the calculations is to test the behavior of the numerical model and not the physics of the specific cosmological models, time is scaled to $u_0 = 1$ and geometric coordinates are used to provide dimensionless results. In all cases the numerical results (points in the figures) closely follow the transformed results (lines in the figures). Table I gives a summary of the test cases.

The radial extent of the results are the maximum values for which the calculations were found to be stable on a regular grid. The region most interesting for the current investigation is that around the AH, which is well within the domain of calculation and, therefore special techniques to extend the radial boundaries were not considered. The maximum value for u was taken to be the oldest PNC where the calculations were stable beyond the AH of that particular PNC. In comparison with the results in [17], in which the diameter distance was used as the radial coordinate, significant improvements in the region covered were obtained. In terms of the redshift z, in the EdS case the maximum value obtained in [17] was $z = 0.99$ on a reduced u region, and the results in Fig. 5 of [17] were for $z = 0.47$ and $z = 0.48$ for the EdS and LTB models, respectively.[4] These values have now been extended to $z = 4.5$ and $z = 1.2$ for EdS and LTB, respectively, in both cases well beyond the location of the AH (which is z at $r_{\max}$ in Table I).

Figure 7(b) is a particularly interesting illustration of an observer's perception of distance in an inhomogeneous universe. Here, the ($\hat{r}$, z) behavior on earlier PNCs includes

[4]In the figures in [17], $u_{\max}$ refers to the u value of a PNC originating from the comoving t value at the AH. E.g. for the EdS model $u_{\max} = 8/27$, which is the t value at the AH. In this paper, $u_{\max}$ refers directly to the maximum u value considered.

loops, which will completely obscure the perception of diameter distance and redshift as measures of distance. This type of behavior provides insight into the physical nature of a model by investigating its past behavior. Although the initial PNC of the specific LTB model is not significantly out of line compared to more accepted models, especially on low redshifts, its past behavior is rather unusual. This does not make it unrealistic, but does say that an observer at $u = u_{\max}$ would have found the interpretation of cosmological data particularly difficult.

1. Einstein-de Sitter

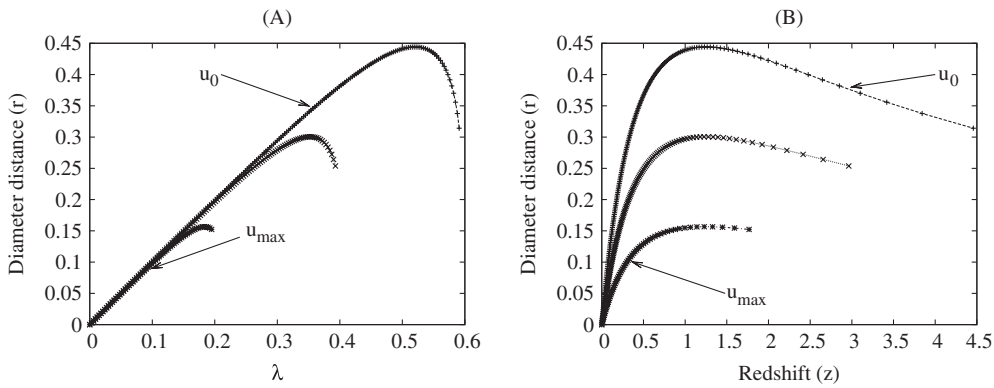

FIG. 3. Diameter distance against λ (A) and against of z (B) on PNCs at different proper times (u) evolved from a local PNC up to $z = 4.5$.

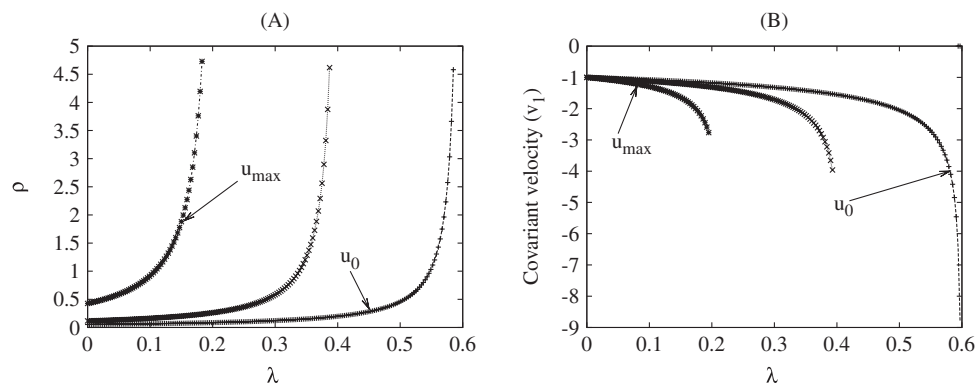

FIG. 4. Density distribution (A) and covariant velocity (B) on PNCs at different proper times (u) evolved from a local PNC up to $z = 4.5$.

2. ΛCDM *with* $\Omega_\Lambda = 0.7$

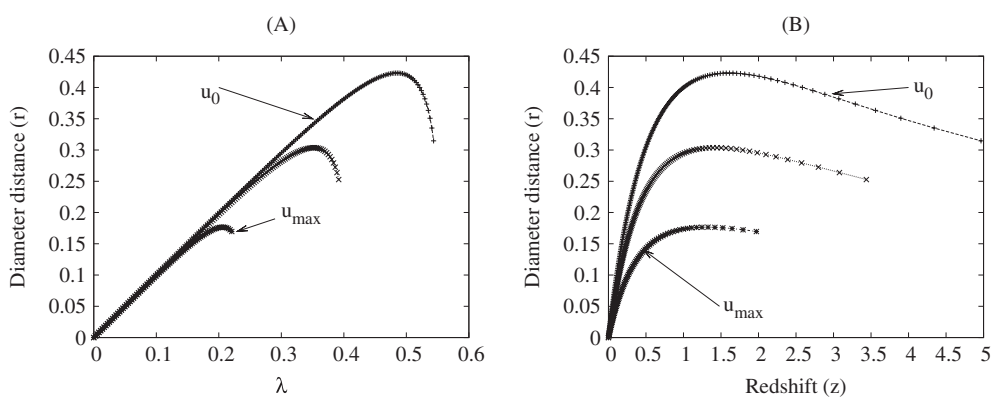

FIG. 5. Diameter distance against λ (A) and against of z (B) on PNCs at different proper times (u) evolved from a local PNC up to $z = 5$.

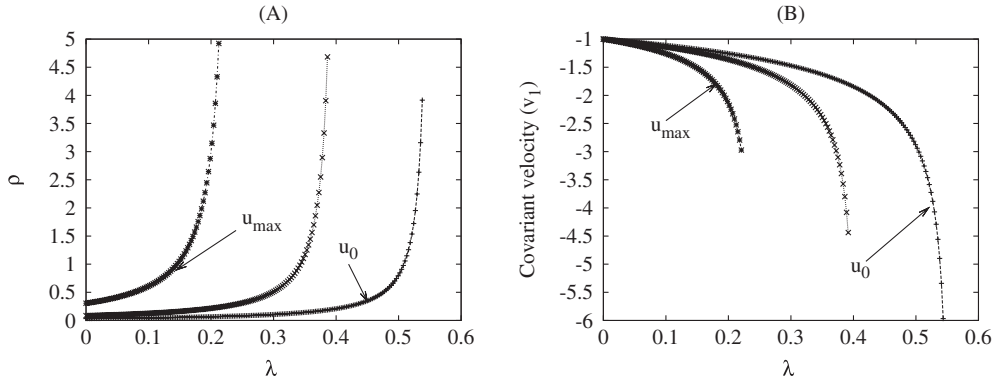

FIG. 6. Density distribution (A) and covariant velocity (B) on PNCs at different proper times (u) evolved from a local PNC up to $z = 5$.

3. LTB with $b = -0.5$

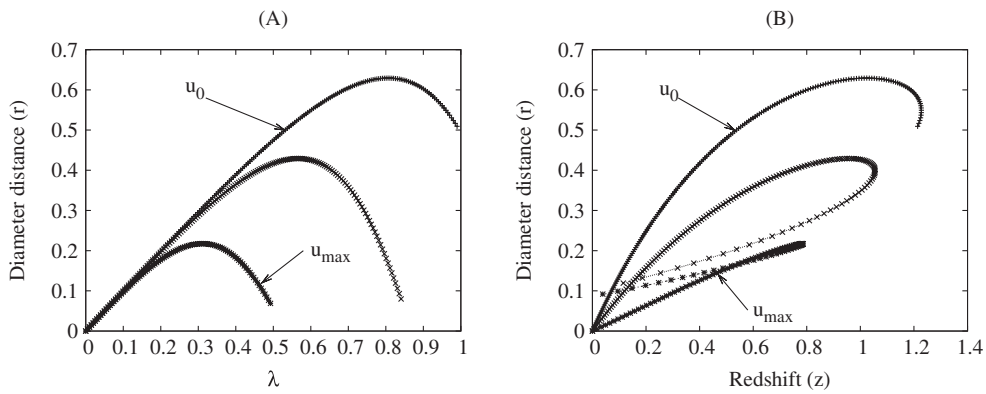

FIG. 7. Diameter distance against λ (A) and against of z (B) on PNCs at different proper times (u) evolved from a local PNC up to $z = 1.2$.

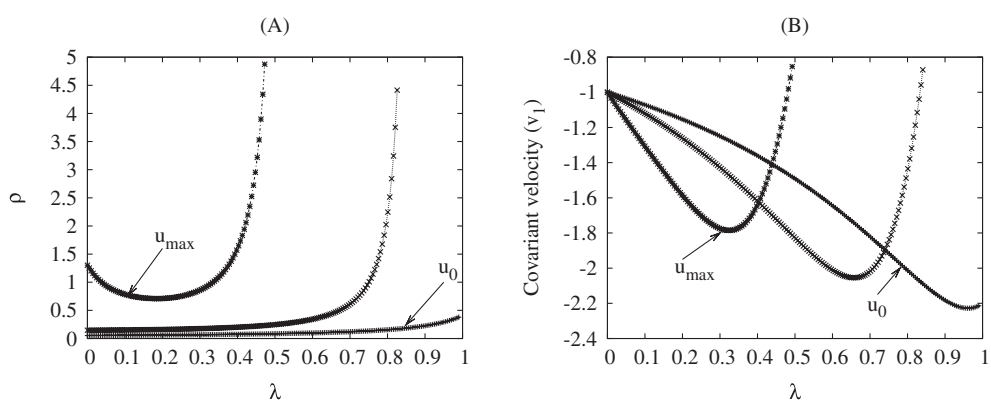

FIG. 8. Density distribution (A) and covariant velocity (B) on PNCs at different proper times (u) evolved from a local PNC up to $z = 1.2$.

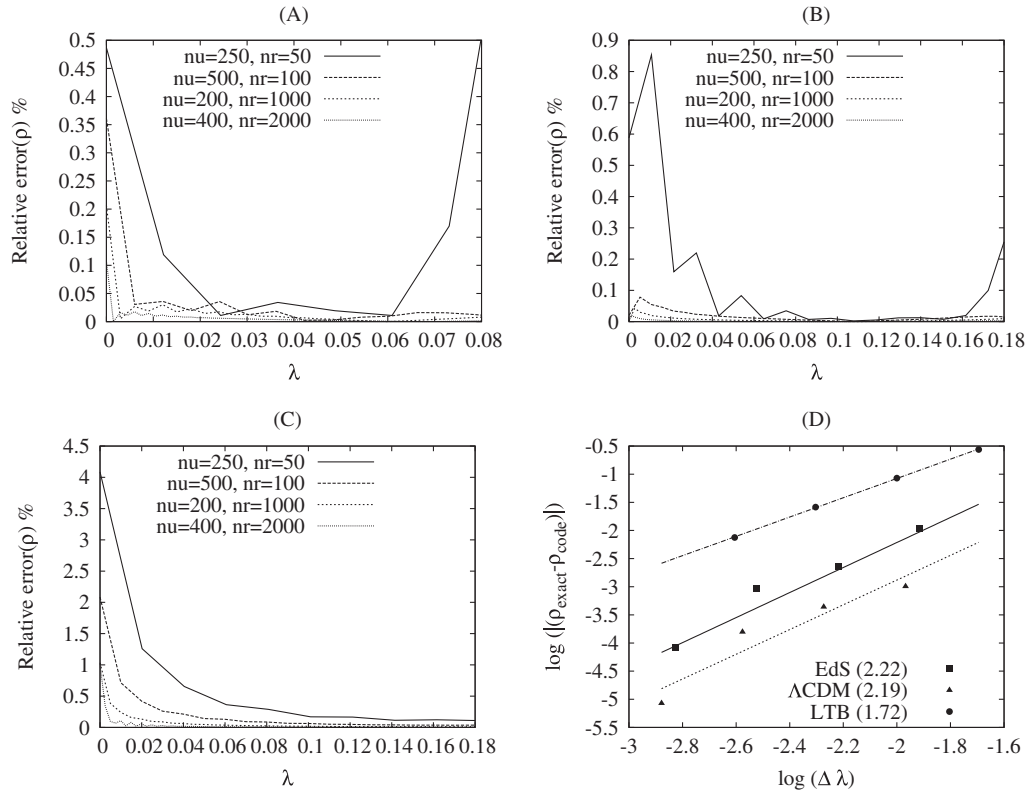

FIG. 9. Radial error distribution on the oldest null cones for the Einstein-de Sitter ($u_{\max} = 0.35$) (A), ΛCDM ($u_{\max} = 0.4$) (B), and LTB ($u_{\max} = 0.2$) (C) models for different grid resolutions. In (D), the error against grid size is shown; the slope of the change in error represents the order of convergence and is indicated in brackets in the legend.

B. Convergence and accuracy

Figures 9(a)–9(c) show the error propagation between the numerical calculations and the transformed results for different grid resolutions. Although the error values are generally small, it is visible that close to $\lambda = 0$, where series expansions are used, the local error values are higher. No specific techniques were employed to reduce these errors, since this provides an indication of the model's stability to local errors. The convergence of errors are general and on higher grid resolutions the difference in error values are less evident.

Figure 9(d), displays the convergence behavior of the calculations. Comparing the error size of the ρ calculations with the grid size, gives the order of convergence between 1.7 and 2.2, i.e. around second-order convergence. Since no specific techniques were used to balance the error sizes in the series expansion calculations with the CIVP calculations, the models also shows good convergence sensitivity against local errors. This effect will be investigated in detail in the future to determine how the model will behave with initial data with realistic observational error margins.

VI. CONCLUSION

The ideal observational approach proposed in [1] can arguably be considered the most philosophically sound approach to cosmology since it only studies the part of the Universe that is causally connected to a cosmological observer. Practically, a very precise map of the contents of the universe is required to develop the full potential of this approach, which, even in the era of precision cosmology, is not yet achievable. The more conventional model-based approach is therefore, and will probably for some time, still be the most favorable approach for assessing our understanding of the Universe. However, the model and observational approaches do not have to be advocated in opposition since restricted implementations of the observational approach can provide insight into the question: Can our conventional understanding of the Universe, which is based on *a priori* assumptions such as the Copernican principle, be derived from less restrictive models making only the most essential assumptions?

The affine CIVP model developed in this paper provides a numerical implementation of the observational approach restricted to a dust filled isotropic universe. The model is particularly well suited for investigating the historic evolution of the observable universe as a reversed CIVP evolved from observations on a local PNC. The line element of the affine CIVP, is closely related to the Bondi-Sachs metric, which makes it a direct process to adapt existing numerical schemes to the new metric. As

with the standard characteristic formalism, second-order convergence and accuracy was achieved when verified against models with known solutions. Similar to the simulations in [17], this provides a useful mechanism to investigate the physical consistency of cosmological models given identical observations on the observer PNC. With the standard characteristic formalism, this could only be implemented in the region prior to the AH, with the affine CIVP the region is extended far enough to investigate the effect of the cosmological constant on the history of the observable universe.

ACKNOWLEDGMENTS

This work was supported by the National Research Foundation, South Africa.

[1] G. F. R. Ellis, *et al.*, Phys. Rep. **124**, 315 (1985).
[2] J.-P. Uzan, C. Clarkson, and G. F. R. Ellis, Phys. Rev. Lett. **100**, 191303 (2008).
[3] C. Hellaby and A. H. A. Alfedeel, Phys. Rev. D **79**, 043501 (2009).
[4] G. Temple, *Royal Society of London Proceedings Series A* 168, 122 (1938).
[5] M. E. Araújo and W. R. Stoeger, Phys. Rev. D **60**, 104020 (1999).
[6] M. E. Araújo and W. R. Stoeger, Phys. Rev. D **80**, 123517 (2009).
[7] M. E. Araújo and W. R. Stoeger, Phys. Rev. D **82**, 123513 (2010).
[8] M. E. Araújo and W. R. Stoeger, J. Cosmol. Astropart. Phys. 7 (2011) 029.
[9] N. Mustapha, C. Hellaby, and G. F. R. Ellis, Mon. Not. R. Astron. Soc. **292**, 817 (1997).
[10] N. Mustapha, B. A. C. C. Bassett, C. Hellaby, and G. F. R. Ellis, Classical Quantum Gravity **15**, 2363 (1998).
[11] T. Hui-Ching Lu and C. Hellaby, Classical Quantum Gravity **24**, 4107 (2007).
[12] M. L. McClure and C. Hellaby, Phys. Rev. D **78**, 044005 (2008).
[13] N. T. Bishop, *et al.*, Phys. Rev. D **56**, 6298 (1997).
[14] J. Winicour, Living Rev. Relativity **12**, 3 (2009).
[15] C. Reisswig, *et al.*, Phys. Rev. Lett. **103**, 221101 (2009).
[16] N. T. Bishop and P. Haines, Quaest. Math. **19**, 259 (1996).
[17] P. J. van der Walt and N. T. Bishop, Phys. Rev. D **82**, 084001 (2010).
[18] C. Hellaby, Mon. Not. R. Astron. Soc. **370**, 239 (2006).
[19] H. Bondi, Nature (London) **186**, 535 (1960).
[20] H. Bondi, M. G. J. van der Burg, and A. W. K. Metzner, *Royal Society of London Proceedings Series A* 269, 21 (1962).
[21] R. K. Sachs, *Royal Society of London Proceedings Series A* 270, 103 (1962).
[22] G. F. R Ellis, in *Relativistic Cosmology*, edited by R. K. Sachs, General Relativity and Cosmology, Proc. Int. School of Physics 'Enrico Fermi' (Varenna), Course XLVII (Academic Press, Waltham, Massachusetts, 1971), p. 104–179.Gen. Relativ. Gravit. **41**, 581 (2009).
[23] L. Pasquini, *et al.*, The Messenger **140**, 20 (2010).
[24] N. T. Bishop, *et al.*, Phys. Rev. D **60**, 024005 (1999).
[25] R. L. Burden and J. D. Faires, *Numerical Analysis* (PWS Publishing Company, Boston, 1993), fifth ed..
[26] G. F. R. Ellis and H. van Elst, *Cosmological Models, Cargèse lectures* (Kluwer, Dordrecht, The Netherlands, 1998); in *NATO ASIC Proc. 541: Theoretical and Observational Cosmology* (Kluwer, Dordrecht, The Netherlands, 1999), pp. 1–116.
[27] M. B. Ribeiro, Astrophys. J. **441**, 477 (1995).
[28] O. Lahav and Y. Suto, Living Rev. Relativity **7**, 11 (2004).
[29] G. Lemaître, Annales de la Société Scientifique de Bruxelles **53**, 51 (1933).For an English translation see: The Expanding Universe. Gen. Relativ. Gravit. **29**, 641 (1997).
[30] R. C. Tolman, Proc. Nat. Acad., Sci. 20, 169 (1934).
[31] H. Bondi, Mon. Not. R. Astron. Soc. **107**, 410 (1947).
[32] M.-N. Célérier, Astron. Astrophys. **353**, 63 (2000).
[33] J.-F. Pascual-Sánchez, Mod. Phys. Lett. A **14**, 1539 (1999).
[34] K. Enqvist, Gen. Relativ. Gravit. **40**, 451 (2007).
[35] J. Garcia-Bellido and T. Haugbølle, J. Cosmol. Astropart. Phys. 4 (2008) 003.
[36] M.-N. Célérier, arXiv:astro-ph/0702416.
[37] J. Plebański and A. Krasiński, *An Introduction to General Relativity and Cosmology* (Cambridge University Press, Cambridge, England, 2006), first ed.
[38] M. E. Araújo and W. R. Stoeger, Mon. Not. R. Astron. Soc. **394**, 438 (2009).